Silver Nanowires on Carbon Nanotube Aerogel Sheets for Flexible, Transparent Electrodes

Patricia M. Martinez [1, 2], Arthur Ishteev [3, 4], Azin Fahimi [†, 5], Josef Velten [1], Izabela Jurewicz [5], Alan B. Dalton [6], Steve Collins[1, 2] Ray H. Baughman [1, 2] and Anvar A. Zakhidov[, 1, 3, 4]*

1 University of Texas at Dallas, NanoTech Institute, Richardson, TX, 75080, United States.

2 University of Texas at Dallas, Department of Chemistry, Richardson, TX 75080, United states.

3 National University of Science and Technology, MISiS, Leninskiy prospect, Moscow, 119049, Russia.

4 ITMO University, 49 Kronverksky Pr. St. Petersburg, 197101, Russia.

5 University of Surrey, Guildford, Surrey GU2 7XH, United Kingdom.

6 University of Sussex, Falmer, Brighton BN1 9RH, United Kingdom.

KEYWORDS: Silver nanowires, multiwall carbon nanotubes, percolation, conductive, transparent electrode, free-standing electrode.

ABSTRACT: Flexible, free-standing transparent conducting electrodes (TCEs) with simultaneously tunable transmittances up to 98% and sheet resistances down to 11 Ω/sq were prepared by a facile spray-coating method of silver nanowires (AgNWs) onto dry-spun multiwall

carbon nanotube (MWNT) aerogels. Counterintuitively, the transmittance of the hybrid electrodes can be increased as the mass density of AgNWs within the MWNT aerogels increases, however, the final achievable transmittance depends on the initial transparency of the MWNT aerogels. Simultaneously, a strong decrease in sheet resistance is obtained when AgNWs form a percolated network along the MWNT aerogel. Additionally, anisotropic reduction in sheet resistance and polarized transmittance of AgNW/MWNT aerogels is achieved with this method. The final AgNW/MWNT hybrid TCEs transmittance and sheet resistance can be fine-tuned by spray-coating mechanisms or by choosing initial MWNT aerogel density. Thus, a wide range of AgNW/MWNT hybrid TCEs with optimized optoelectronic properties can be achieved depending of the requirements needed. Finally, the free-standing AgNW/MWNT hybrid TCEs can be laminated onto a wide range of substrates without the need of a bonding aid.

1. Introduction

The need to find materials for replacing Indium Tin Oxide (ITO) in flexible transparent conducting electrodes (TCEs) has stimulated the search for low-cost, lightweight alternatives that have high transparency and electrical conductivity, high mechanical strength, and are compatible with the numerous substrates used in optoelectronic devices. Though ITO combines high optical transmittance (>90% at 550 nm) with low sheet resistance (10 Ω/sq)[1], applications of ITO-based flexible electrodes are limited by the scarcity of indium and the inherent brittleness of metal oxides[2,3]. Novel technologies, such as for ITO nanowires[4] and ITO mesh structures prepared via photolithography[5], have been developed to prevent ITO from cracking. However, the fabrication of such flexible ITO TCEs requires complex and expensive processes[1,4]. Efforts have been made to develop flexible TCEs based on multi-walled carbon nanotubes (MWNTs)[6–8], single-walled carbon nanotubes[6,9–16], graphene[17–20], and a combination of the above[3,10,21,22] as alternatives to

ITO[6]. Of particular interest are free-standing MWNT aerogels sheets that can be drawn in the dry state from the side of spinnable MWNT forests[23]. These highly oriented aerogels sheets are porous, transparent, flexible, and conducting. When exposed to organic solvents, like isopropyl alcohol (IPA) or methanol, they densify during solvent evaporation, reducing sheet thickness from ~20 μm to ~50 nm. MWNT aerogels can also be laminated to a wide range of substrates by making contact in the desired section with an organic solvent and allowing surface tension effects during evaporation to densify the aerogel, increasing the contact area between MWNTs and the substrate[23]. However, these self-supported aerogels are highly electronically and optically anisotropic, which can be an undesired property for optoelectronic devices.

Though the use of carbon-based nanomaterials improves the flexibility of TCEs, their low conductivity and transmittance limits optoelectronic performance[24]. Their comparatively high sheet resistances and low transmittances make them unsuitable when choices optical transmittance above 90 % and sheet resistance below 100 Ω/sq is required[25,26]. Thus, substantial optical and electrical improvements are necessary for carbon-based nanomaterials to become viable TCEs alternatives.

By integrating silver nanowires (AgNWs) with carbon-based nanomaterials, hybrid TCEs having low sheet resistances and high transmittances, similar to ITO, can be realized[27,28]. The optical and electrical properties of these hybrid TCEs improve when AgNWs percolation networks are formed, increasing the number of conduction pathways connecting AgNWs either to themselves or to the carbon nanomaterial[26,29,30]. These hybrid TCEs provide direct proportionality between sheet resistance and transmittance, as the amount of AgNWs deposited defines the maximum sheet resistance that can be obtained without losing transparency of the substrate[26]. Previous studies have shown that AgNWs can be easily combined with carbon

nanomaterials by spray-coating, spin coating, drop-casting, or roll-coating to form hybrid TCEs[3,17,36–44,18,19,21,31–35]. Of these techniques, spray-coating is the most suitable and scalable technique since it can be used over large volumes with high reproducibility, while insuring homogeneous AgNWs distributions[30,45].

Typically, AgNWs-carbon hybrid TCEs deploy polyethylene terephthalate (PET)[46–49], polyethylene naphthalate (PEN)[6], or polydimethylsiloxane (PDMS)[50] as the flexible substrate and receive a post-treatment to further optimize the transmittance and sheet resistance . Post-treatments, including thermal annealing[51,52], mechanical pressing[53], photophysical welding[50,54], low energy plasma[55], and electrochemical Ostwald ripening processes[56] are quite successful, but require fabricating the hybrid electrodes separated from the optoelectronic devices to prevent damage of the layers. Free-standing TCEs that can be laminated onto any device layer have been developed for single-component-based materials, such as metallic AgNWs networks[57], graphene films[58], single-walled carbon nanotubes[59] or MWNT aerogels[23]. In contrast, most of the reported hybrid carbon/metal TCEs are substrate-supported. Hence, it would be valuable to fabricate free-standing AgNWs-carbon based hybrids that meet industrial requirements for TCEs and could be laminated onto any substrate surface.

In this work, free-standing carbon/metal hybrid TCEs are produced in which the optical, electrical and mechanical properties of dry-spun MWNT aerogels are combined with the attributes of AgNWs. To avoid the trade-off between transmittance and sheet resistance, free-standing MWNT aerogels are spray-coated with a solution of AgNWs in IPA. This results in simultaneous increase in transmittance and decrease in sheet resistance as the density of AgNWs increases within the MWNT aerogel. During the process of MWNT aerogel densification by evaporating organic solvents, apertures greater than the wavelength of light ($\lambda_{\text{visible light}}$), form in

the aerogel, increasing overall transmittance. Also, relying on the high thermal conductivity of MWNT aerogels[60], the contact resistance of the AgNWs is reduced when a fast 1–2 minute thermal annealing process is performed. As a result, free-standing AgNW/MWNT hybrids with sheet resistances ~11 Ω/sq and transmittances ~98 % are produced that can be laminated onto targeted substrates. Thus, the described technology produces AgNW/MWNT hybrid TCEs that exceed industrial requirements for TCEs in optoelectronic devices.

2. Experimental Section

2.1. Materials. Two types of AgNWs suspensions, AgNWs-25 and AgNWs-60 with concentrations of 5 mg/mL in isopropyl alcohol (IPA) were purchased from Seashell Technologies. The mean lengths were 30 μm and 15 μm, with mean diameter of 25 nm and 60 nm, respectively. The AgNWs solutions were diluted to a concentration of 0.25 mg/mL with IPA prior to spray coating. AgNWs-130 with diameters between 50–150 nm and lengths greater than 20 μm were synthesized by a polyol method, described by Vinogradov et al[61].

2.2. Silver evaporation. A 10 nm thick layer of silver was evaporated onto MWNT aerogels with a CHA-50 electron beam evaporator at a rate of 1.2–1.7 Å/sec. Prior to Ag deposition, the MWNT aerogels were vapor-densified with IPA.

2.3. Synthesis of MWNT aerogels. Free standing MWNT aerogels were drawn from the sidewall of a spinnable MWNT forest synthesized by chemical vapor deposition (CVD)[23]. The substrates were prepared by depositing 3 nm of iron catalyst using an electron beam (CHA-50) onto Si wafers bearing 100 nm of silicon oxide. A mixture of acetylene (116.8 sccm) and hydrogen (1354 sccm) in a He (2400 sccm) atmosphere were reacted with the substrates at temperatures between 700–730˚C for 5–10 min.

2.4. Preparation of the AgNW/MWNT aerogels. Dry-spun MWNT aerogels were placed on the top of the sheet supports having a 1x1 inch rectangular aperture in the middle and copper (Cu) tape electrodes at the edges, see Figure 1a. To measure the MWNT aerogel anisotropic sheet resistance, Rs, the Cu electrodes were positioned in a parallel (||) and perpendicular (⊥) manner with respect to the horizontally oriented MWNTs electrically conductive path. In a || configuration, the Cu electrodes were placed along the less resistive MWNT aerogel path, whereas in the ⊥ configuration, the Cu electrodes were placed along the higher aerogel resistive path, see Figure 1b. Silver paste was painted on top of the contact between the MWNT aerogels and the copper electrodes to ensure sound electrical connection. The Rs of the aerogel films were calculated using:

$$Rs = Resistance\left(\frac{MWNT\ aerogel\ lenght}{MWNT\ aerogel\ width}\right)$$

The transmittances of the aerogel for 550-nm-light polarized ⊥ and || to the MWNT direction were measured using the polarization mode of a UV-Vis spectrometer (Perkin Elmer Lambda 900 UV-Vis/NIR Spectrophotometer).

Before spray coating the MWNT aerogels with the AgNWs solution, the pristine MWNT aerogels were vapor densified[23] using IPA. To accomplish this, 100 mL of IPA was placed in a 500 mL beaker, covered with aluminum foil, and heated on a hot plate at 95˚C for 5 minutes to produce IPA vapors. The aerogels were placed in the beaker (facing down 2–10 cm from the liquid IPA) for 5–30 seconds, and then slowly lifted from the beaker to avoid breakage, see Figure 1c–d. A Paasche SI airbrush, which was connected to an Argon or Nitrogen gas source, was used to deposit the AgNWs onto the aerogel at a set pressure of 40 psi, see Figure 1e. The airbrush was maintained vertically during the entire spray coating process and moved from left to right to ensure uniform coverage of the MWNT aerogel. The distance between the brush nozzle

and MWNT aerogels was set at 20–30 cm. Every 20 passes, the sprayed aerogels were placed on a hot plate at 95˚C for 5 minutes to complete evaporation of the IPA from the MWNT aerogels. Afterwards, resistance and transmittance measurements were made, as previously described. Thermal annealing at 160˚C on a hot plate for 1–2 minutes was performed to decrease the non-effective contacts between AgNWs within the MWNT aerogels and to evaporate any organic solvent residues, see Figure 1f.

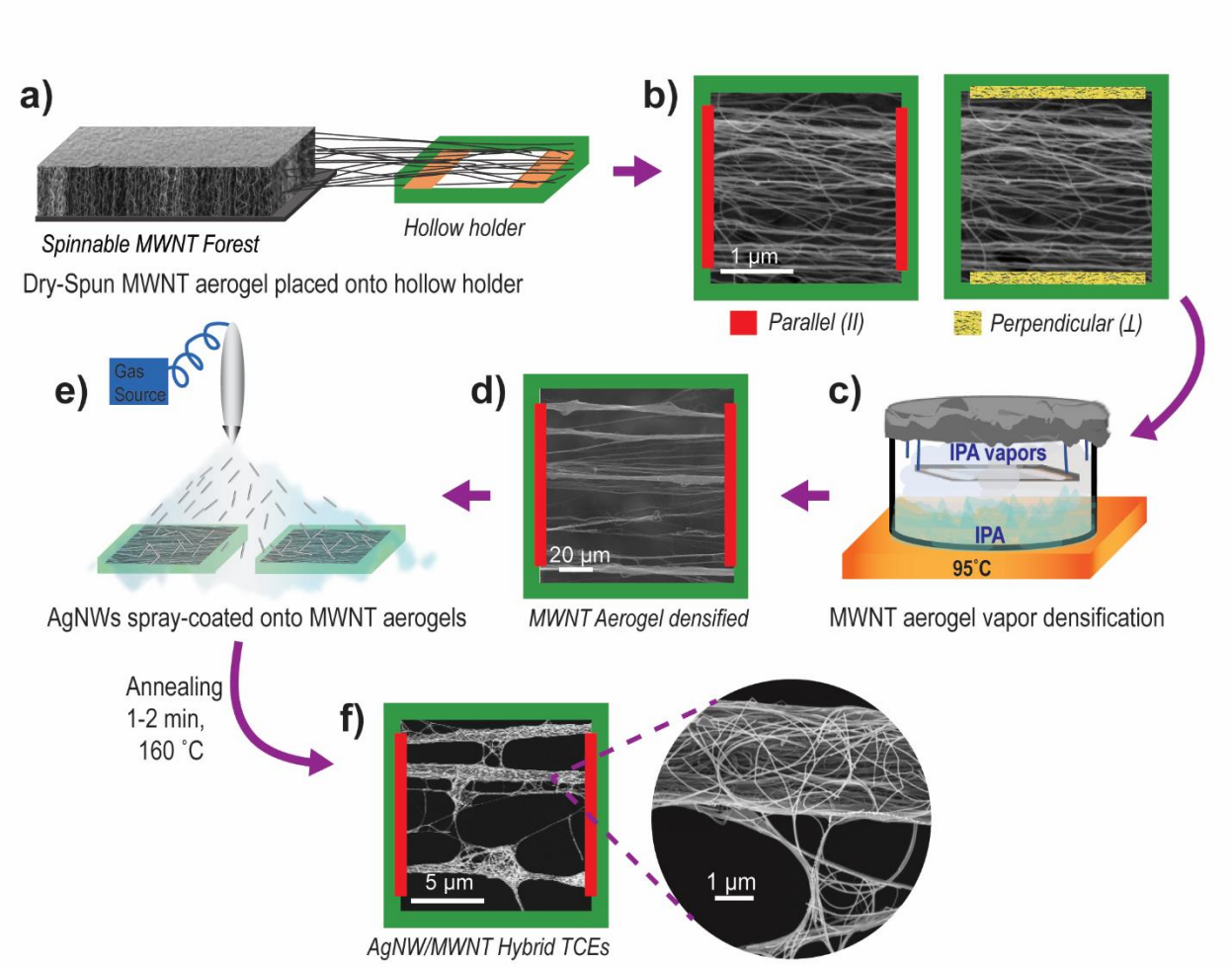

Figure 1. Preparation of flexible AgNW/MWNT hybrid TCEs. a) MWNT aerogel dry-spun on top of a hollow holder. b) MWNT aerogel parallel and perpendicular configurations. c) Densification of the MWNT aerogels with IPA vapors and d) the morphology of the MWNT

aerogel after vapor densification. e) Spray-coating AgNWs onto the perpendicular and parallel MWNT aerogel configurations and f) AgNW/MWNT hybrid TCE morphology after thermal annealing.

2.5. MWNT aerogel areal density. MWNT aerogel areal density was calculated by dividing the weight of one MWNT aerogel sheet by its area. Using measured weights of 4, 6, 8 and 10 MWNT aerogel sheets, linear regression analysis was used to predict the weight of a single aerogel. The weight of the aerogel sheets was an average of three measurements recorded with a microgram accurate scale. To minimize human error, dimensions of the sheets (width and length) were obtained using an optical microscope with attached camera and analyzed using MatLab to obtain an estimation of the area.

2.6. Physical characterization. AgNW/MWNT aerogels morphologies were characterized using a scanning electron microscope, SEM (Zeiss-LEO Model 1530 Variable Pressure Field Effect Scanning Electron Microscope) and a transmittance electron microscope, TEM (JEOL 2100F).

3. Results and discussion

Figure 2a is a photograph showing the transparency of an AgNW/MWNT hybrid TCE that was spray-coated with a 0.25 mg/mL solution of AgNWs and then thermally annealed. This hybrid TCE, which provided $T(\perp)$ = 98.9 % and Rs ($\parallel$)= 11 Ω/sq, is flexible (Figure S1a–b in Supporting Information), self-supporting and can be transferred to a wide range of substrates (glass, polymer, metal, etc.) without the aid of an adhesive layer. Unless otherwise indicated, the AgNW/MWNT hybrid TCEs transmittance is perpendicular transmittance, $T(\perp)$, taken at 550nm and the sheet resistance is parallel sheet resistance, Rs($\parallel$).

Figure 2b shows the increase in transmittance and reduction of Rs, as the amount of deposited AgNWs increases within MWNT aerogels. It highlights the three enhancing mechanisms; Densification Effect, AgNWs Effect, and Thermal Annealing Effect, which occur when spray-coating MWNTs aerogels with AgNWs/IPA solution.

The first enhancement mechanism, labeled as Densification Effect, is responsible for increasing the transmittance of the AgNW/MWNT hybrid TCEs to values > 90 %, and initially reducing the Rs by ~30%. Here AgNWs account for a negligible percentage of the total decrease in Rs since a percolated AgNWs system has not been achieved[29]. The initial decrease in Rs occurs when the solvent densifies, or reduces the aerogel initial thickness from ~20 μm to ~50 nm, creating stronger contacts between individual nanotubes[23]. SEM imaging in Figure 2c depicts the Densification Effect mechanism that occur when fine droplets of AgNWs/IPA locally wet the MWNT aerogel and IPA surface tension forces develop between parallel MWNTs strands, pushing them into thicker bundles with diameters ≤ 5 μm. As the IPA solvent evaporates, strong van der Waals forces develop between individual nanotubes within the bundles allowing them to remain collapsed and create apertures greater than $\lambda_{\text{visible light}}$, Figure 2d. While the solvent is being evaporated from the MWNT aerogel, AgNWs carried by the solvent droplets are deposited on top or between the newly formed MWNT bundles. A significant reduction of the aerogel's Rs is recorded only when the number of AgNWs reach the electrical percolation threshold. At this point, AgNWs have formed enough connecting paths with themselves, other AgNWs and/or with MWNT bundles through which electrons can travel. The effect of a simultaneous increase in transmittance and decrease in Rs does not occur when porous polymers, such as electrospun Polyacrylonitrile (PAN) nanofiber aerogel membranes, are spray-coated with AgNWs in exactly same way as for MWNT aerogels. In PAN electrospun

membranes, the Rs can be lowered (Rs final in the kΩ range) by the formation of the AgNWs conductive network around and between the apertures of the PAN fibers, in the same way that occurs in MWNTs aerogels. Because PAN fibers do not experience strong Van-der Waals bundling under surface tension forces when in contact with IPA, and its initial morphology prevents for the opening of apertures for increased light transmission, the overall transmittance decreases (contrary to the increase in MWNT aerogels) as the amount of AgNWs spray-coated to the PAN membranes increases, Figure S3a–d.

Once the AgNWs electrical percolation threshold is achieved within the MWNT aerogel, the second enhancement mechanism, labeled as AgNWs Effect in Figure 2b, takes place and the formation of the AgNWs conductive network begins. In this region, solvent densification increases the transmittance ~0.1 % while Rs continues to decrease rapidly as more AgNWs are deposited onto the MWNT aerogel until reaching a maximum decrease in Rs of 70 %. Figure 2e portrays the final morphology of the AgNW/MWNT electrode after the AgNW network is formed. The apertures between adjacent MWNT bundles with dimensions greater than $\lambda_{\text{visible light}}$ that allow the enhanced light transmission of the AgNW/MWNT hybrid TCE are mainly formed during the Densification Effect but the AgNW conductive network, depicted in Figure 2f, is created during the AgNWs Effect. New electrical pathways are formed when AgNWs wrap around and connect MWNT bundles as well as when AgNWs connect with themselves and other AgNWs to form the AgNW conductive network lowering the Rs of the AgNW/MWNT electrode.

The Rs of the AgNW/MWNT hybrid TCE is further lowered during the third enhancement mechanism; the Thermal Annealing Effect a 1–2minute thermal annealing process at 160˚C. This quick annealing takes advantage of the high thermal conductivity of the MWNTs[60] to reduce the

non-effective contacts between AgNWs and decrease by 50 % the Rs of the AgNW/MWNT hybrids TCEs. It also evaporates any organic solvent residues from the spray-coating[52] mechanism. Figure 2g and Figure S4a–b, show the effectiveness of this quick annealing where the AgNWs are welded to one another at the contact points without disrupting the MWNT aerogel. Overheating above the ideal temperature or for prolonged lengths of time drastically increases the Rs of the AgNW/MWNT hybrid TCEs due to fragmentation of AgNWs into shorter wires or by disintegration of AgNWs into Ag droplets, Figure S4c–d.

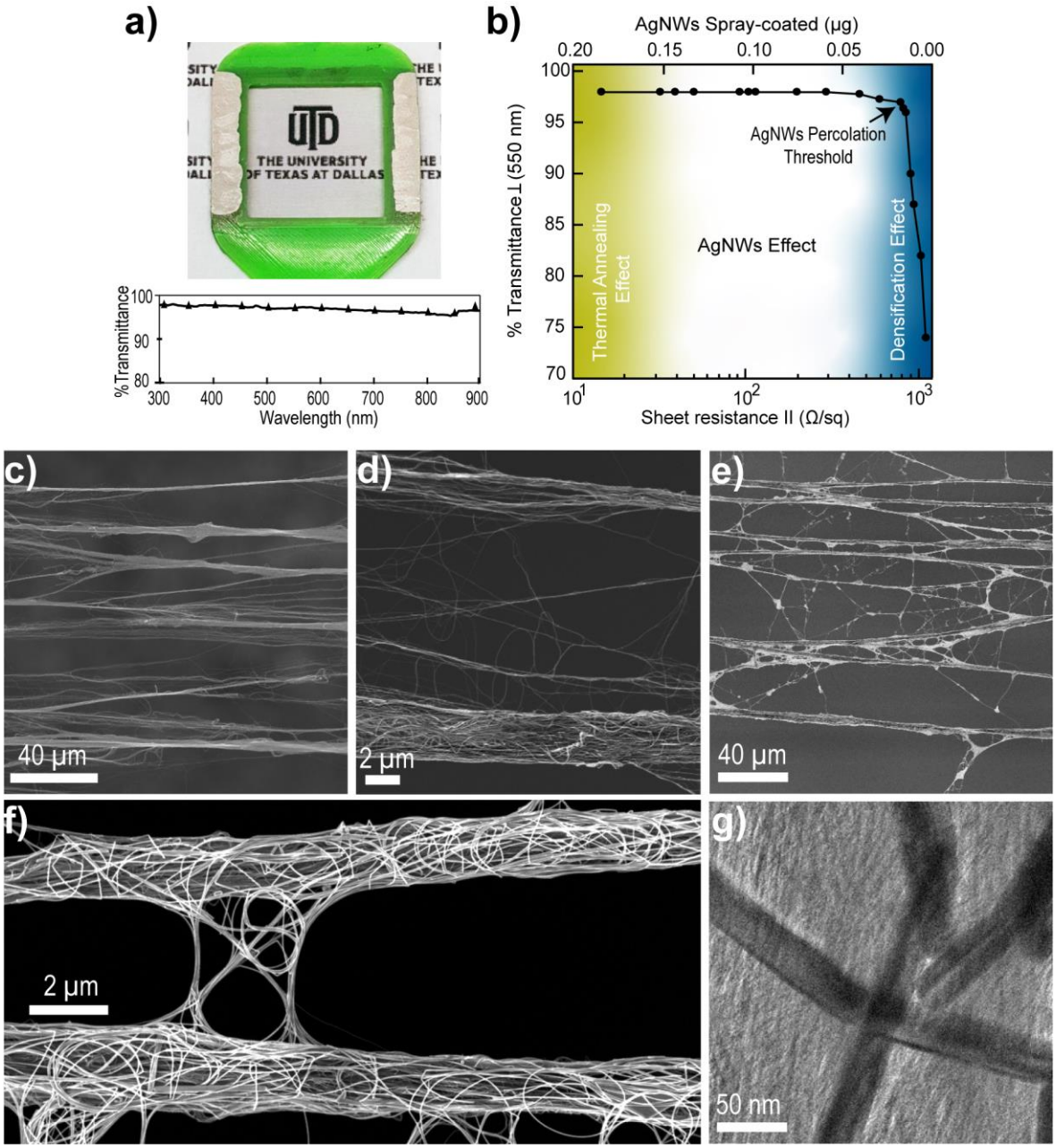

Figure 2. a) AgNW/MWNT hybrid TCE with T(⊥)= 98 % and Rs(||)= 11.0 Ω/sq. b) AgNW/MWNT aerogel increase in T(⊥) and Rs(||) reduction representing the three enhancing mechanisms occurring during spray-coating of AgNWs/IPA; Densification Effect, AgNWs Effect, and Thermal Annealing Effect. c) SEM image showing the MWNT aerogel morphology after Densification Effect and d) collapsed MWNT bundles with apertures greater than $\lambda_{\text{visible light}}$.

e) SEM image depicting the AgNW/MWNT network and f) close-up of the AgNW network formed between two MWNT bundles. g) TEM image of AgNWs welded to one another after Thermal Annealing Effect.

3.1 Optical and electrical anisotropic behavior

Dry-spun MWNT aerogels are anisotropic by nature due to the preferential alignment of nanotubes along the pulling direction. Therefore, it is expected that their optical and electrical anisotropic behavior changes when spray-coated with the AgNWs/IPA solution. A suppression of anisotropic polarized transmittance, TA, along ‖ and ⊥ nanotube direction, is reduced when TA= ‖/⊥ quotient is close to unity. From Figure 3a, the AgNW/MWNT hybrid TCEs behave as a transparent isotropic material when TA increases from 0.38 to 0.99 as a consequence of MWNT aerogel apertures greater than $\lambda_{\text{visible light}}$ formed during the Densification Effect.

The anisotropic behavior of Rs, defined as Rs_A= Rs(‖)/Rs(⊥), , is reduced when the AgNWs electrical percolation threshold is achieved and continues to be reduced until the AgNWs conductive network is stablished. The Rs_A quotient close to unity reflects a total loss of anisotropic resistance behavior and represents electrons equally percolating through the AgNW/MWNT hybrid in the ‖ and ⊥ MWNT directions. Before spray-coating the MWNT aerogels with the AgNWs/IPA solution, the initial aerogel Rs(⊥) is ~70 fold higher than Rs (‖), leading to an Rs_A=0.20. After spray-coating 0.180 ± 0.10 μg of AgNWs, the maximum amount needed to achieve the lowest Rs, a ~2.5 fold difference between Rs(⊥) and Rs(‖) is recorded as Rs_A=0.40 is achieved, see Figure 3b. Rs(⊥) is the limiting factor in the Rs_A equation. For Rs(⊥) to have a value similar to Rs(‖), AgNWs need to connect adjacent MWNTs bundles and arrange

a conductive network in the perpendicular direction, requiring AgNWs with lengths ≥ MWNT aerogel apertures.

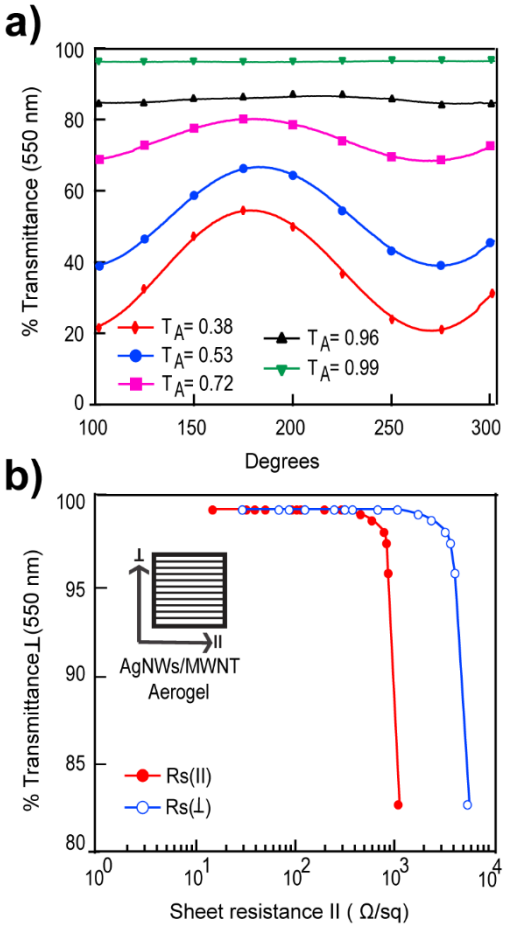

Figure 3. a) Suppression of anisotropic transmittance, TA, taken at 550 nm while the light source rotated from 100 to 300 degrees. A maximum transmittance is obtained when $\overrightarrow{E_{field}}$ is ⊥ to the MWNTs direction while a minimum is achieved when is $\overrightarrow{E_{field}}$ || to the MWNTs direction. A lost in anisotropic polarization transmittance is achieved when the transmittance anisotropic quotient, TA= ||/⊥, increased from 0.38 to 0.99, corresponding to the sinusoidal graph profile loss. b) Plot of T(⊥) at 550 nm vs Rs in the || and ⊥ MWNTs direction. The Rs

anisotropic behavior, Rs_A, is reduced when the quotient, Rs(||)/Rs(⊥), increased from 0.20 to 0.40 corresponding to a final Rs(||)= 11.0 Ω/sq and Rs (⊥)= 29.2 Ω/sq, after annealing treatment.

3.2 AgNWs dimension effects

AgNWs lengths and diameters affect the onset of the AgNWs electrical percolation threshold, the formation of the AgNWs conductive network and thus, the overall Rs of the AgNW/MWNT hybrid TCEs. Figure 4a, plots the transmittance versus Rs of three types of AgNWs with different diameters and lengths spray-coated onto MWNT aerogels. Also shown in this figure is the effect of spraying exclusively with IPA, outlining the decrease in Rs and increase in transmittance due to the Densification Effect. The highest decrease in Rs is obtained when AgNWs-25 with diameters ~22 nm and lengths ~18 µm are used, Figure 4a, (blue triangles). These AgNWs are flexible enough that, when sprayed, wrap around individual MWNT bundles, creating more opportunities to connect with themselves or with other AgNWs and long enough to form bridges between adjacent MWNT bundles; both are properties well suited to create the AgNWs conductive network and effectively reduce the Rs ~ 70% after densification, Figure 4c and Figure S5a–b.

On the contrary, AgNWs-60 with diameters ≥ 40 nm and short lengths < 10µm, when sprayed to the MWNT aerogels, form non-optimal AgNWs networks and decrease the overall Rs ~10% after densification, Figure 4a, black squares. These AgNWs appear to be rigid and lay atop the MWNT bundles without wrapping around them, forming few bridges between adjacent MWNTs when AgNWs agglomeration occur, Figure 4d and Figure S5c–d. If the length of the AgNWs is ≥ 18 µm and a diameter ≥ 40 nm is maintained (AgNWs-130), a 50% decrease in Rs is seen after

densification, Figure 4a (red circles). In this case, AgNWs interconnect neighboring MWNT bundles, without wrapping around them, Figure 4e and Figure S5e–f.

High values of transmittances can be obtained regardless of the type of AgNWs sprayed onto the MWNT aerogels because the increase of AgNWs/MWNT TCEs transmittance is solely affected by the MWNT aerogel's solvent densification and is independent of AgNWs dimensions. The inverse proportionality between transmittance and Rs, is only observed when MWNT aerogels are sprayed-coated with an AgNWs/IPA solution, and not when silver is evaporated onto MWNT aerogels or when AgNWs/IPA are spray-coated onto glass slides. Silver evaporated onto a MWNT aerogel is a solvent-free technique and spray-coating AgNWs onto glass is unaffected by densification mechanisms thus, transmittance and Rs decrease linearly as the amount of deposited silver increases, see Figure 4b.

A summary of the lowest Rs achieved for each type of AgNWs sprayed onto MWNT aerogels, and when Ag is evaporated on top of MWNTs is presented in Table 1.

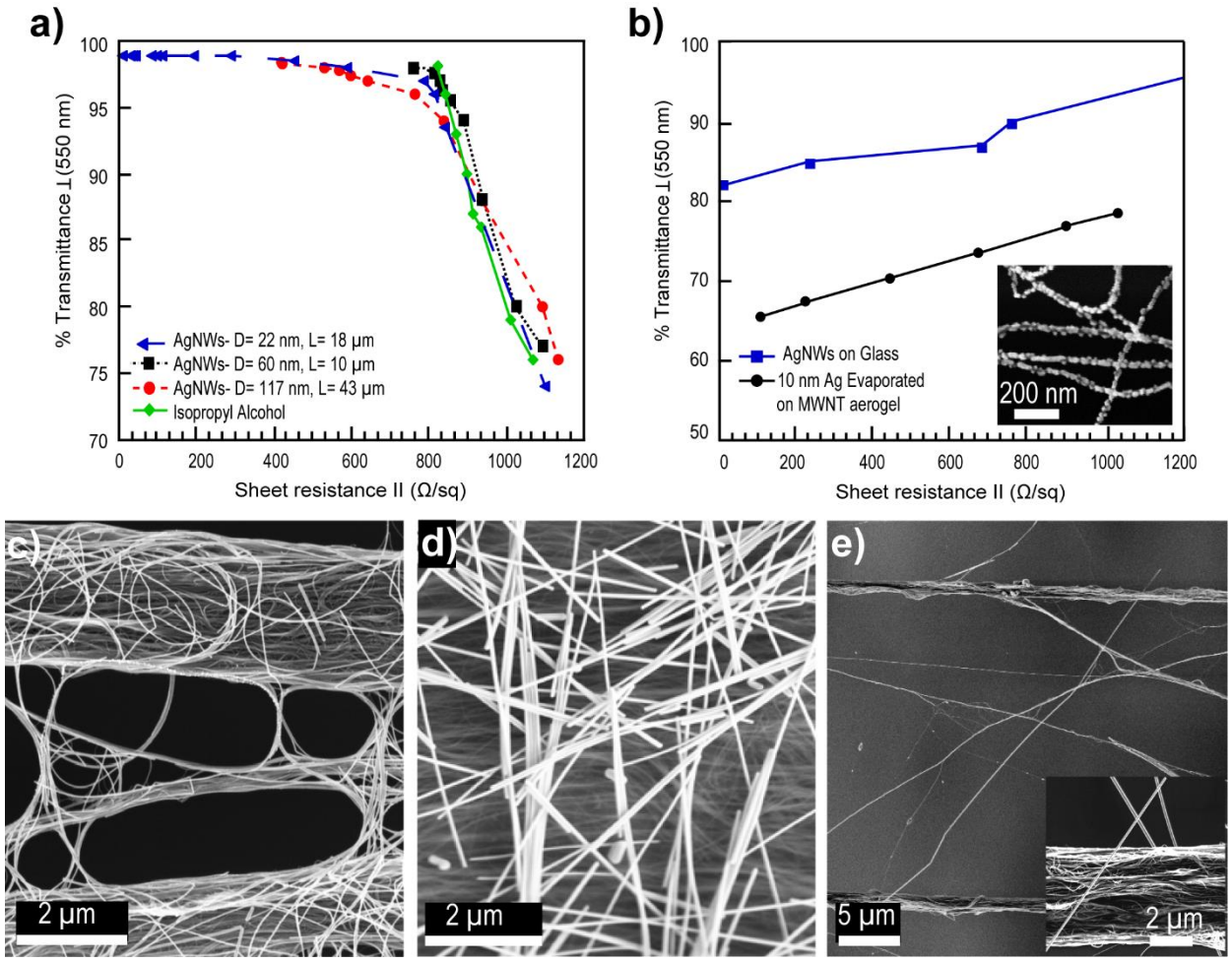

Figure 4. a) Evolution of MWNT aerogels increase in transmittance and decrease in Rs when spray-coated with AgNWs with different diameters and lengths. The effect of spraying MWNT aerogels with IPA is plotted as a reference. Linear decrease in transmittance and Rs is observed for b) 10 nm of Ag e-beam evaporated onto a MWNT aerogel, black circles and for AgNWs-25 with small diameters (22 nm) and medium lengths (18 µm), are spray-coated to a glass slide, blue squares. Morphology of MWNT aerogel with 10 nm of Ag evaporated is shown as an inset. SEM of c) AgNWs-25 with small diameters (22 nm) and medium lengths (18 µm) wrapping and connecting neighbor MWNT bundles and d) AgNWs-60 with medium diameters (60 nm) and short lengths (10 µm) laying on top of a MWNT bundle. e) AgNWs-130 with large diameters

(117 nm) and large lengths (43 μm) laying on top of a MWNT bundle without wrapping around it. All the SEM images are taken at the lowest Rs achieved before annealing.

Table 1. Effect of AgNW dimensions

AgNW/MWNT Hybrid TCEs MWNTs/( )	**Ave. Diameter (nm)**	**Ave. Length (μm)**	**T(⊥) max (%)**	**Rs(‖) min (Ω/sq)**
(AgNWs-25)	22	18	98	11
(AgNWs-60)	60	10	98	789
(AgNWs-130)	117	43	98	420
(Ag evaporated)	-	-	67	95
***AgNWs-25 on glass**	22	18	82	7

3.3. MWNTs aerogel density effect

MWNT aerogel density plays an important role in constraining the maximum transmittance and minimum Rs, in the ⊥ and ‖ direction, that the AgNW/MWNT hybrids can reach. Ideally, low AgNWs network densities are desired to reduce the optical haze of the hybrid TCEs and still obtain low Rs and high transmittances[29]. Although long and thin AgNWs are required to form ideal AgNWs conductive networks necessary to lower the Rs, MWNT aerogel areal density limits the amount of AgNWs per unit area needed to reach the lowest Rs and highest transmittance. Aerogels with high areal densities ~ 5.6 μg/cm^2, have initial low transmittances, T= 53 ± 5 % and nominal sheet resistances, and Rs= 410 ± 25 Ω/sq. These aerogels require a low AgNWs mass density of ~ 20.6 μg/cm^2 to obtain a Rs ~10 Ω/sq after annealing, with final T~ 90 %. For MWNT aerogels with low areal densities ~2.8 μg/cm^2, the initial Rs and transmittances

are 825 ± 50 Ω/sq and 70 ± 10 %, respectively. With a AgNWs mass density of ~50.0 µg/cm^2, these MWNT aerogels can achieve Rs ~11 Ω/sq after annealing; values similar to MWNT aerogels with high areal density, but on the contrary, transmittances as high as 99 % can be achieved, see Figure 5.

A tradeoff between MWNT aerogel areal density and AgNWs mass density exists that greatly influences the optical and electrical properties of the AgNW/MWNT hybrid TCEs. Since low MWNT aerogel areal densities have less CNTs/cm^2, when densified with the AgNWs/IPA solution, thinner bundles and bigger apertures are formed allowing the transmittance to achieve values > 90 %. The lower < 90 % transmittance, seen in MWNT aerogels with high areal densities is a consequence of more CNTs/cm^2 available to form additional and/or thicker MWNT bundles when densified, creating apertures lower than the $\lambda_{\text{visible light}}$ that absorb or reflect the incident light more efficiently.

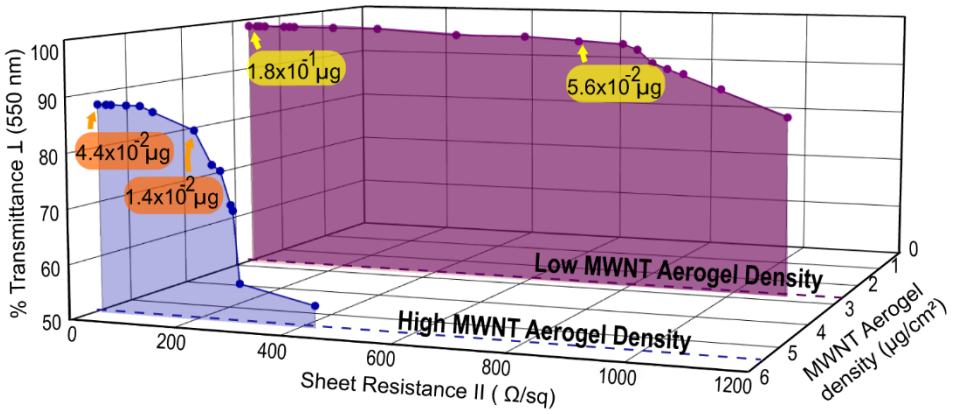

Figure 5. Transmittance ⊥ (550 nm) versus sheet resistance || plotted as a function of MWNT aerogel areal density indicating the amount of AgNWs spray-coated (µg) After the percolation threshold was reached.

4. Conclusion

In this study, hybrid and self-supported TCEs made of AgNWs spray-coated onto MWNT aerogels have proven to achieve simultaneous increase in transmittances above 90 % and decrease in Rs below 15 Ω/sq by in situ formation of micro-sized MWNT aerogel apertures and deposition of AgNWs. AgNWs with small diameters (22 nm) and medium lengths (18 μm) were found to create ideal AgNWs conductive networks when spray-coated to MWNT aerogels by wrapping around MWNT bundles, creating effective connections with themselves and with neighboring MWNT bundles. MWNT aerogel Rs and transmittance anisotropic behavior was also suppressed by the formation of apertures with sizes larger than the wavelength of light and by creating new electrical pathways when AgNWs connected neighboring MWNT bundles. The reduced electrical anisotropy is desired for many applications in optoelectronics where charge injection or collection from the transparent electrode is expected to be uniform and isotropic in all directions.

MWNT aerogels with areal densities similar to or below 2.8 $\mu g/cm^2$, were found to be the most suitable aerogels for AgNWs deposition due to their intrinsic high transmittance. However, the high sheet resistance of these low-density aerogels required a greater amount of AgNWs ~50 $\mu g/cm^2$ to achieve low Rs. Of great interest is the ability to fine tune the amount of AgNWs needed within the MWNT aerogel needed to achieve the percolation critical point. This suggests further research to achieve an optimal balance of AgNWs and MWNTs in order to maximize the desirable properties of this system as a new form of TCE. In addition, these materials can easily be transferred onto various substrates, making them applicable to a wide variety of technologies within the flexible electronics field and allowing for applications not possible with traditional TCEs that are currently available.

AUTHOR INFORMATION

Corresponding Author

* Corresponding author. Tel: 972-883-6218. Email: zakhidov@utdallas.edu (Anvar Zakhidov)

Present Addresses

† California Institute of Technology, 1200 East California Boulevard, Pasadena, California 91125, United States.

Author Contributions

All authors have given approval to the final version of the manuscript.

Funding Sources

Patricia M. Martinez received partial financial support from the Mexican Concejo Nacional de Ciencia y Tecnología (CONACYT). Patricia M. Martinez and Josef Velten received funding from Welch Foundation of Texas via grant AT-1617 and Navy STTR Marcorp N181-002-1004. Arthur Istheev received founding from the Ministry of Science and Higher Education of the Russian Federation via grant No K2-2019-014 and Partial financial support from the Ministry of Education and Science of the Russian Federation, Grant No 14.Y26.31.0010.

ACKNOWLEDGEMENTS

The authors would like to recognize Aldo Garcia-Sandoval for the help with the bending test and Juan Pablo Oviedo for the TEM images.

ABBREVIATIONS

ITO, Indium Thin Oxide; TCEs, Transparent Conducting Electrodes; MWNTs, Multiwall Carbon Nanotube; AgNWs, silver nanowires; Rs, sheet resistance; T, Transmittance; CVD, Chemical Vapor Deposition.

Associated content

Supporting information available: Bending test for the AgNWs/MWNT hybrid TCEs on PDMS substrates. TEM images of contacts between AgNWs and MWNTs and SEM images of AgNW/MWNT TCEs after ideal and beyond ideal thermal annealing conditions. SEM images depicting the morphology of AgNW/MWNT TCEs spray coated with different AgNWs-25, AgNWs-60 and AgNWs-130. SEM images of Polyacrylonitrile (PAN) membranes spray-coated with AgNWs-25.

REFERENCES

(1) Lin, H. K.; Hsu, W. C. Electrode Patterning of ITO Thin Films by High Repetition Rate Fiber Laser. *Appl. Surf. Sci.* **2014**, *308*, 58–62.

(2) Alzoubi, K.; Hamasha, M. M.; Lu, S.; Sammakia, B. Bending Fatigue Study of Sputtered ITO on Flexible Substrate. *J. Disp. Technol.* **2011**, *7* (11), 593–600.

(3) Peng, L.; Feng, Y.; Lv, P.; Lei, D.; Shen, Y.; Li, Y.; Feng, W. Transparent, Conductive, and Flexible Multiwalled Carbon Nanotube/Graphene Hybrid Electrodes with Two Three-Dimensional Microstructures. *J. Phys. Chem. C* **2012**, *116* (8), 4970–4978.

(4) Dattoli, E. N.; Lu, W. ITO Nanowires and Nanoparticles for Transparent Films. *MRS Bull.* **2011**, *36* (10), 782–788.

(5) Sakamoto, K.; Kuwae, H.; Kobayashi, N.; Nobori, A.; Shoji, S.; Mizuno, J. Highly Flexible Transparent Electrodes Based on Mesh-Patterned Rigid Indium Tin Oxide. *Sci. Rep.* **2018**, *8* (1), 2825.

(6) Zhou, Y.; Azumi, R. Carbon Nanotube Based Transparent Conductive Films: Progress, Challenges, and Perspectives. *Sci. Technol. Adv. Mater.* **2016**, *17* (1), 493–516.

(7) Sun, J.; Wang, R. Carbon Nanotube Transparent Electrode. In *Syntheses and Applications of Carbon Nanotubes and Their Composites*; 2013.

(8) Aloui, W.; Ltaief, A.; Bouazizi, A. Transparent and Conductive Multi Walled Carbon Nanotubes Flexible Electrodes for Optoelectronic Applications. *Superlattices Microstruct.* **2013**, *64*, 581–589.

(9) Jiang, S.; Hou, P. X.; Chen, M. L.; Wang, B. W.; Sun, D. M.; Tang, D. M.; Jin, Q.; Guo, Q. X.; Zhang, D. D.; Du, J. H.; Tai, K. P.; Tan, J.; Kauppinen, E. I.; Liu, C.; Cheng, H. M. Ultrahigh-Performance Transparent Conductive Films of Carbon-Welded Isolated Single-Wall Carbon Nanotubes. *Sci. Adv.* **2018**, *4* (5), eaap9264.

(10) Hecht, D. S.; Hu, L.; Irvin, G. Emerging Transparent Electrodes Based on Thin Films of Carbon Nanotubes, Graphene, and Metallic Nanostructures. *Adv. Mater.* **2011**, *23* (13), 1482–1513.

(11) Doherty, E. M.; De, S.; Lyons, P. E.; Shmeliov, A.; Nirmalraj, P. N.; Scardaci, V.; Joimel, J.; Blau, W. J.; Boland, J. J.; Coleman, J. N. The Spatial Uniformity and Electromechanical Stability of Transparent, Conductive Films of Single Walled Nanotubes. *Carbon N. Y.* **2009**, *47* (10), 2466–2473.

(12) Tenent, R. C.; Barnes, T. M.; Bergeson, J. D.; Ferguson, A. J.; To, B.; Gedvilas, L. M.; Heben, M. J.; Blackburn, J. L. Ultrasmooth, Large-Area, High-Uniformity, Conductive Transparent Single-Walled-Carbon-Nanotube Films for Photovoltaics Produced by Ultrasonic Spraying. *Adv. Mater.* **2009**, *21* (31), 3210–3216.

(13) Hu, L.; Hecht, D. S.; Gruner, G. Percolation in Transparent and Conducting Carbon

Nanotube Networks. *Nano Lett.* **2004**, *4* (12), 2513–2517.

(14) Blackburn, J. L.; Barnes, T. M.; Beard, M. C.; Kim, Y.-H. H.; Tenent, R. C.; McDonald, T. J.; To, B.; Coutts, T. J.; Heben, M. J. Transparent Conductive Single-Walled Carbon Nanotube Networks with Precisely Tunable Ratios of Semiconducting and Metallic Nanotubes. *ACS Nano* **2008**, *2* (6), 1266–1274.

(15) Wu, Z.; Chen, Z.; Du, X.; Logan, J. M.; Sippel, J.; Nikolou, M.; Kamaras, K.; Reynolds, J. R.; Tanner, D. B.; Hebard, A. F.; Rinzler, A. G. Transparent, Conductive Carbon Nanotube Films. *Science (80-.).* **2004**, *305* (5688), 1273–1276.

(16) Tokuno, T.; Nogi, M.; Jiu, J.; Suganuma, K. Hybrid Transparent Electrodes of Silver Nanowires and Carbon Nanotubes: A Low-Temperature Solution Process. *Nanoscale Res. Lett.* **2012**, *7* (1), 281.

(17) Wassei, J. K.; Kaner, R. B. Graphene, a Promising Transparent Conductor. *Mater. Today* **2010**, *13* (3), 52–59.

(18) Tung, V. C.; Allen, M. J.; Yang, Y.; Kaner, R. B. High-Throughput Solution Processing of Large-Scale Graphene. *Nat. Nanotechnol.* **2009**, *4* (1), 25–29.

(19) Wang, X.; Zhi, L.; Müllen, K. Transparent, Conductive Graphene Electrodes for Dye-Sensitized Solar Cells. *Nano Lett.* **2008**, *8* (1), 323–327.

(20) Eda, G.; Fanchini, G.; Chhowalla, M. Large-Area Ultrathin Films of Reduced Graphene Oxide as a Transparent and Flexible Electronic Material. *Nat. Nanotechnol.* **2008**, *3* (5), 270–274.

(21) Jurewicz, I.; Fahimi, A.; Lyons, P. E.; Smith, R. J.; Cann, M.; Large, M. L.; Tian, M.; Coleman, J. N.; Dalton, A. B. Insulator-Conductor Type Transitions in Graphene-Modified Silver Nanowire Networks: A Route to Inexpensive Transparent Conductors.

Adv. Funct. Mater. **2014**, *24* (48), 7580–7587.

(22) Kholmanov, I. N.; Magnuson, C. W.; Piner, R.; Kim, J. Y.; Aliev, A. E.; Tan, C.; Kim, T. Y.; Zakhidov, A. A.; Sberveglieri, G.; Baughman, R. H.; Ruoff, R. S. Optical, Electrical, and Electromechanical Properties of Hybrid Graphene/Carbon Nanotube Films. *Adv. Mater.* **2015**, *27* (19), 3053–3059.

(23) Zhang, M.; Fang, S.; Zakhidov, A. A.; Lee, S. B.; Aliev, A. E.; Williams, C. D.; Atkinson, K. R.; Baughman, R. H. Strong, Transparent, Multifunctional, Carbon Nanotube Sheets. *Science (80-.).* **2005**, *309* (5738), 1215–1219.

(24) Luo, M.; Liu, Y.; Huang, W.; Qiao, W.; Zhou, Y.; Ye, Y.; Chen, L. Sen. Towards Flexible Transparent Electrodes Based on Carbon and Metallic Materials. *Micromachines* **2017**, *8* (1), 12.

(25) Ackermann, T.; Neuhaus, R.; Roth, S. The Effect of Rod Orientation on Electrical Anisotropy in Silver Nanowire Networks for Ultra-Transparent Electrodes. *Sci. Rep.* **2016**, *6*, 34289.

(26) Lagrange, M.; Langley, D. P.; Giusti, G.; Jiménez, C.; Bréchet, Y.; Bellet, D. Optimization of Silver Nanowire-Based Transparent Electrodes: Effects of Density, Size and Thermal Annealing. *Nanoscale* **2015**, *7* (41), 17410–17423.

(27) Liang, J.; Li, L.; Tong, K.; Ren, Z.; Hu, W.; Niu, X.; Chen, Y.; Pei, Q. Silver Nanowire Percolation Network Soldered with Graphene Oxide at Room Temperature and Its Application for Fully Stretchable Polymer Light-Emitting Diodes. *ACS Nano* **2014**, *8* (2), 1590–1600.

(28) Ricciardulli, A. G.; Yang, S.; Wetzelaer, G.-J. J. A. H.; Feng, X.; Blom, P. W. M. Hybrid Silver Nanowire and Graphene-Based Solution-Processed Transparent Electrode for

Organic Optoelectronics. *Adv. Funct. Mater.* **2018**, *28* (14), 1706010.

(29) Langley, D. Silver Nanowire Networks : Effects of Percolation and Thermal Annealing on Physical Properties, 2014.

(30) Bellet, D.; Lagrange, M.; Sannicolo, T.; Aghazadehchors, S.; Nguyen, V. H.; Langley, D. P.; Muñoz-Rojas, D.; Jiménez, C.; Bréchet, Y.; Nguyen, N. D. Transparent Electrodes Based on Silver Nanowire Networks: From Physical Considerations towards Device Integration. *Materials (Basel).* **2017**, *10* (6).

(31) Lee, J. Y.; Connor, S. T.; Cui, Y.; Peumans, P. Solution-Processed Metal Nanowire Mesh Transparent Electrodes. *Nano Lett.* **2008**, *8* (2), 689–692.

(32) De, S.; Higgins, T. M.; Lyons, P. E.; Doherty, E. M.; Nirmalraj, P. N.; Blau, W. J.; Boland, J. J.; Coleman, J. N. Silver Nanowire Networks as Flexible, Transparent, Conducting Films: Extremely High DC to Optical Conductivity Ratios. *ACS Nano* **2009**, *3* (7), 1767–1774.

(33) Hu, L.; Kim, H. S.; Lee, J. Y.; Peumans, P.; Cui, Y. Scalable Coating and Properties of Transparent, Flexible, Silver Nanowire Electrodes. *ACS Nano* **2010**, *4* (5), 2955–2963.

(34) Zhu, R.; Chung, C. H.; Cha, K. C.; Yang, W.; Zheng, Y. B.; Zhou, H.; Song, T. Bin; Chen, C. C.; Weiss, P. S.; Li, G.; Yang, Y. Fused Silver Nanowires with Metal Oxide Nanoparticles and Organic Polymers for Highly Transparent Conductors. *ACS Nano* **2011**, *5* (12), 9877–9882.

(35) Garnett, E. C.; Cai, W.; Cha, J. J.; Mahmood, F.; Connor, S. T.; Greyson Christoforo, M.; Cui, Y.; McGehee, M. D.; Brongersma, M. L. Self-Limited Plasmonic Welding of Silver Nanowire Junctions. *Nat. Mater.* **2012**, *11* (3), 241–249.

(36) Maisch, P.; Tam, K. C.; Lucera, L.; Egelhaaf, H.-J. J.; Scheiber, H.; Maier, E.; Brabec, C.

J. Inkjet Printed Silver Nanowire Percolation Networks as Electrodes for Highly Efficient Semitransparent Organic Solar Cells. *Org. Electron. physics, Mater. Appl.* **2016**, *38*, 139–143.

(37) Tokuno, T.; Nogi, M.; Karakawa, M.; Jiu, J.; Nge, T. T.; Aso, Y.; Suganuma, K. Fabrication of Silver Nanowire Transparent Electrodes at Room Temperature. *Nano Res.* **2011**, *4* (12), 1215–1222.

(38) Madaria, A. R.; Kumar, A.; Zhou, C. Large Scale, Highly Conductive and Patterned Transparent Films of Silver Nanowires on Arbitrary Substrates and Their Application in Touch Screens. *Nanotechnology* **2011**, *22* (24), 245201.

(39) Yu, Z.; Zhang, Q.; Li, L.; Chen, Q.; Niu, X.; Liu, J.; Pei, Q. Highly Flexible Silver Nanowire Electrodes for Shape-Memory Polymer Light-Emitting Diodes. *Adv. Mater.* **2011**, *23* (5), 664–668.

(40) Zeng, X. Y.; Zhang, Q. K.; Yu, R. M.; Lu, C. Z. A New Transparent Conductor: Silver Nanowire Film Buried at the Surface of a Transparent Polymer. *Adv. Mater.* **2010**, *22* (40), 4484–4488.

(41) Gaynor, W.; Burkhard, G. F.; McGehee, M. D.; Peumans, P. Smooth Nanowire/Polymer Composite Transparent Electrodes. *Adv. Mater.* **2011**, *23* (26), 2905–2910.

(42) Lee, J.-Y. Y.; Connor, S. T.; Cui, Y.; Peumans, P. Semitransparent Organic Photovoltaic Cells with Laminated Top Electrode. *Nano Lett.* **2010**, *10* (4), 1276–1279.

(43) Gaynor, W.; Lee, J.-Y. Y.; Peumans, P. Fully Solution-Processed Inverted Polymer Solar Cells with Laminated Nanowire Electrodes. *ACS Nano* **2010**, *4* (1), 30–34.

(44) Madaria, A. R.; Kumar, A.; Ishikawa, F. N.; Zhou, C. Uniform, Highly Conductive, and Patterned Transparent Films of a Percolating Silver Nanowire Network on Rigid and

Flexible Substrates Using a Dry Transfer Technique. *Nano Res.* **2010**, *3* (8), 564–573.

(45) Scardaci, V.; Coull, R.; Lyons, P. E.; Rickard, D.; Coleman, J. N. Spray Deposition of Highly Transparent, Low-Resistance Networks of Silver Nanowires over Large Areas. *Small* **2011**, *7* (18), 2621–2628.

(46) Naito, K.; Inuzuka, R.; Yoshinaga, N.; Mei, W. Transparent Conducting Films Composed of Graphene Oxide/Ag Nanowire/ Graphene Oxide/PET. *Synth. Met.* **2018**, *237*, 50–55.

(47) Miao, J.; Chen, S.; Liu, H.; Zhang, X. Low-Temperature Nanowelding Ultrathin Silver Nanowire Sandwiched between Polydopamine-Functionalized Graphene and Conjugated Polymer for Highly Stable and Flexible Transparent Electrodes. *Chem. Eng. J.* **2018**, *345*, 260–270.

(48) Liu, J.; Jiang, T.; Duan, F.; Shen, G.; He, X.; Yang, W.; Liang, P.; Yue, Y.; Lan, Q.; Wu, J.; Zeng, Q. Electrophoresis Deposition of Flexible and Transparent Silver Nanowire/Graphene Composite Film and Its Electrochemical Properties. *J. Alloys Compd.* **2018**, *745*, 370–377.

(49) Chung, W. H.; Park, S. H.; Joo, S. J.; Kim, H. S. UV-Assisted Flash Light Welding Process to Fabricate Silver Nanowire/Graphene on a PET Substrate for Transparent Electrodes. *Nano Res.* **2018**, *11* (4), 2190–2203.

(50) Lee, C.; Oh, Y.; Yoon, I. S.; Kim, S. H.; Ju, B.-K.; Hong, J.-M. Flash-Induced Nanowelding of Silver Nanowire Networks for Transparent Stretchable Electrochromic Devices. *Sci. Rep.* **2018**, *8* (1), 2763.

(51) Radmilović, V. V.; Göbelt, M.; Ophus, C.; Christiansen, S.; Spiecker, E.; Radmilović, V. R. Low Temperature Solid-State Wetting and Formation of Nanowelds in Silver Nanowires. *Nanotechnology* **2017**, *28* (38), 385701.

(52) Langley, D. P.; Lagrange, M.; Giusti, G.; Jiménez, C.; Bréchet, Y.; Nguyen, N. D.; Bellet, D. Metallic Nanowire Networks: Effects of Thermal Annealing on Electrical Resistance. *Nanoscale* **2014**, *6*.

(53) Jing, M. xiang; Han, C.; Li, M.; Shen, X. qian. High Performance of Carbon Nanotubes/Silver Nanowires-PET Hybrid Flexible Transparent Conductive Films via Facile Pressing-Transfer Technique. *Nanoscale Res. Lett.* **2014**, *9* (1), 588.

(54) Pillai, S. K. R.; Wang, J.; Wang, Y.; Sk, M. M.; Prakoso, A. B.; Rusli; Chan-Park, M. B. Totally Embedded Hybrid Thin Films of Carbon Nanotubes and Silver Nanowires as Flat Homogenous Flexible Transparent Conductors. *Sci. Rep.* **2016**, *6* (1), 38453.

(55) Li, J.; Tao, Y.; Chen, S.; Li, H.; Chen, P.; Wei, M. Z.; Wang, H.; Li, K.; Mazzeo, M.; Duan, Y. A Flexible Plasma-Treated Silver-Nanowire Electrode for Organic Light-Emitting Devices. *Sci. Rep.* **2017**, *7* (1), 16468.

(56) Lee, H. J.; Oh, S.; Cho, K. Y.; Jeong, W. L.; Lee, D. S.; Park, S. J. Spontaneous and Selective Nanowelding of Silver Nanowires by Electrochemical Ostwald Ripening and High Electrostatic Potential at the Junctions for High-Performance Stretchable Transparent Electrodes. *ACS Appl. Mater. Interfaces* **2018**, *10* (16), 14124–14131.

(57) Huang, Y.; Bai, X.; Zhou, M.; Liao, S.; Yu, Z.; Wang, Y.; Wu, H. Large-Scale Spinning of Silver Nanofibers as Flexible and Reliable Conductors. *Nano Lett.* **2016**, *16* (9), 5846–5851.

(58) Chen, J.; Guo, Y.; Huang, L.; Xue, Y.; Geng, D.; Liu, H.; Wu, B.; Yu, G.; Hu, W.; Liu, Y.; Zhu, D. Controllable Fabrication of Ultrathin Free-Standing Graphene Films. *Philos. Trans. R. Soc. A Math. Phys. Eng. Sci.* **2014**, *372* (2013), 20130017.

(59) Liu, Q.; Fujigaya, T.; Cheng, H. M.; Nakashima, N. Free-Standing Highly Conductive

Transparent Ultrathin Single-Walled Carbon Nanotube Films. *J. Am. Chem. Soc.* **2010**, *132* (46), 16581–16586.

(60) Aliev, A. E.; Guthy, C.; Zhang, M.; Fang, S.; Zakhidov, A. A.; Fischer, J. E.; Baughman, R. H. Thermal Transport in MWCNT Sheets and Yarns. *Carbon N. Y.* **2007**, *45* (15), 2880–2888.

(61) Vinogradov, V. V.; Felner, I.; Nowik, I.; Avnir, D. Conductive Magnetic Sol-Gel Films. *J. Mater. Chem. C* **2015**, *3* (41), 10723–10727.